

## Supporting Information

### Development of a universal conductive platform for anchoring photo- and electroactive proteins using organometallic terpyridine molecular wires

Margot Jacquet, Miriam Izzo, Silvio Osella, Sylwia Kozdra, Paweł P. Michałowski, Dariusz Gołowicz, Krzysztof Kazimierczuk, Maciej T. Gorzkowski, Adam Lewera, Marian Teodorczyk, Bartosz Trzaskowski, Rafał Jurczakowski, Daniel T. Gryko, Joanna Kargul

#### Table of contents

1. $^1\text{H}$ and $^{13}\text{C}$ NMR spectra of Ligand <b>Lp</b> .....	2
2. Secondary Ion Mass Spectrometry analysis and electrochemical impedance spectroscopy analyses.....	4
3. Purification and biochemical characterisation of His <sub>6</sub> -tagged cytochrome <i>c</i> <sub>553</sub> 19 AA peptide linker variant.....	4
4. X-ray Photoelectron Spectroscopy (XPS) analyses.....	5
5. Cyclic voltammetry analyses.....	6
6. Photochronoamperometric analyses.....	7

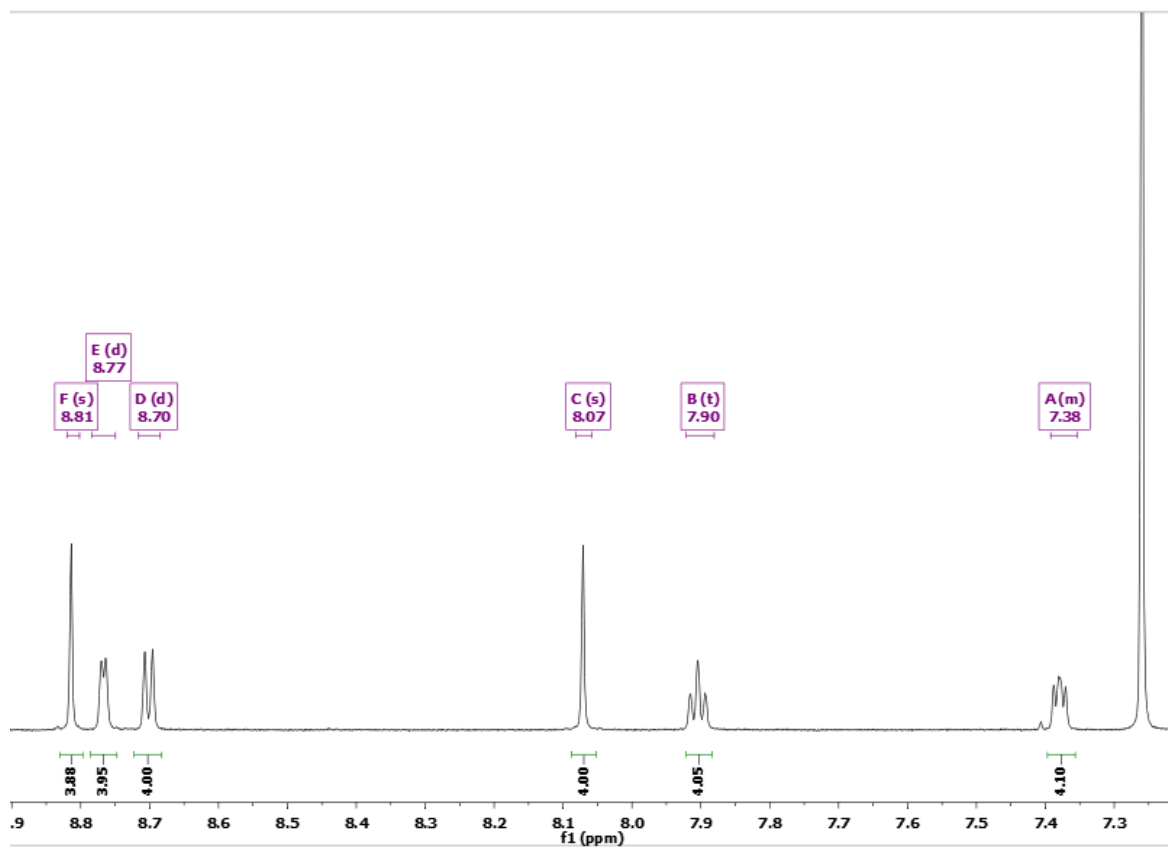


Fig. S1.  $^1H$  NMR in  $CDCl_3$  of the ditopic ligand  $L\phi$ .

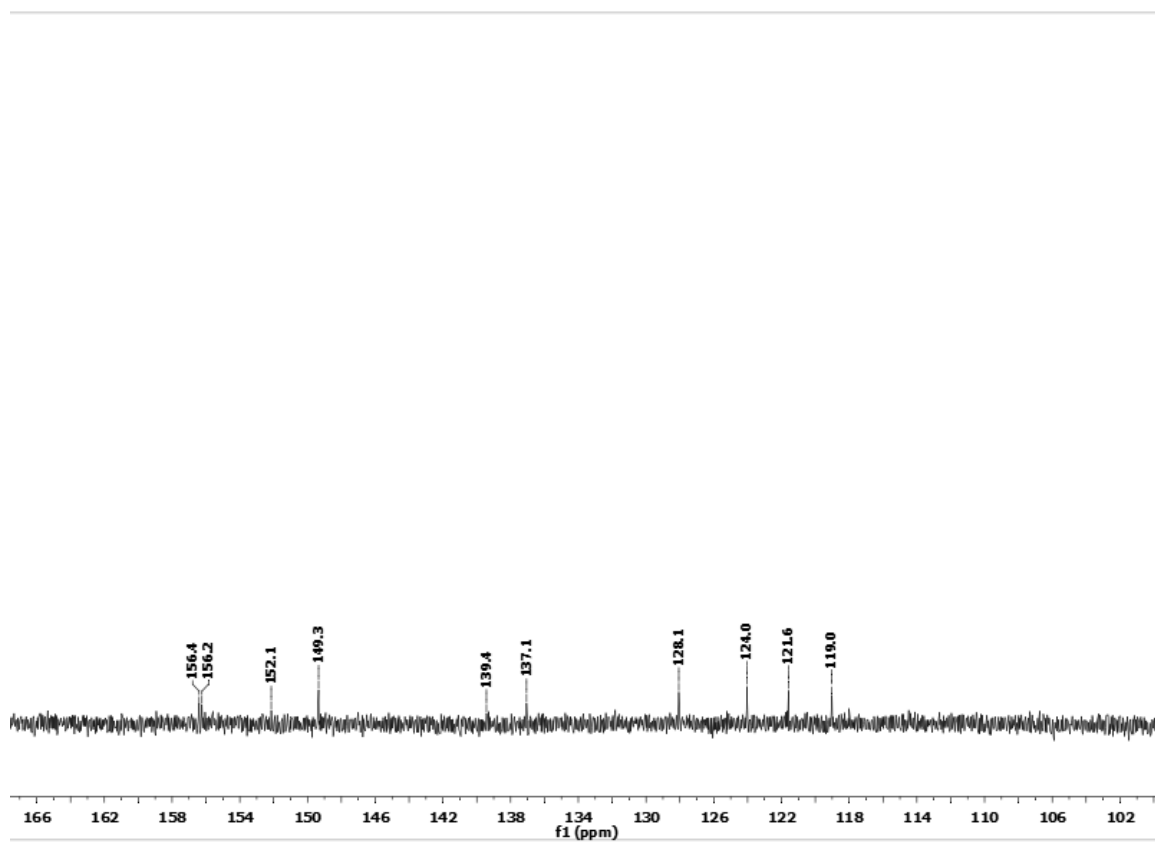


Fig. S2.  $^{13}C$  NMR in  $CDCl_3$  of the ditopic ligand  $L\phi$ .

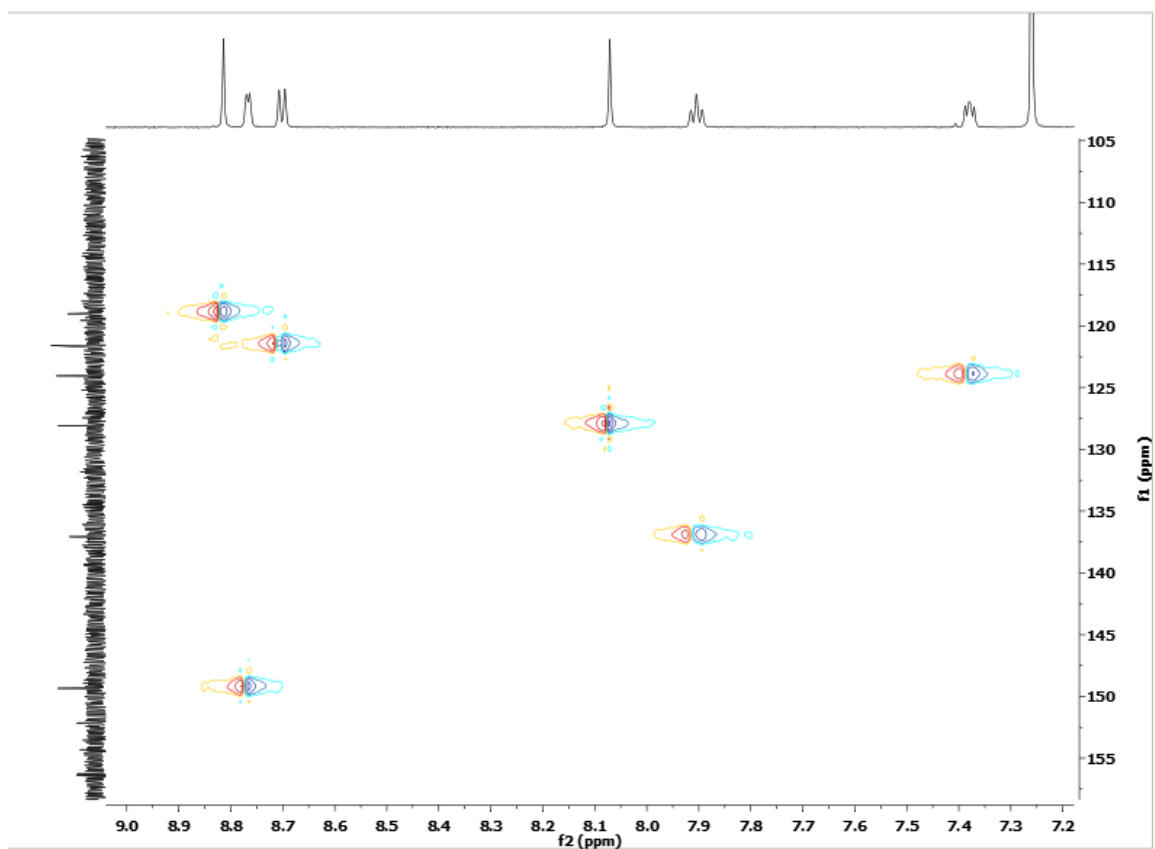


Fig. S3. HSQC NMR in  $\text{CDCl}_3$  of the ditopic ligand  $\text{L}\phi$ .

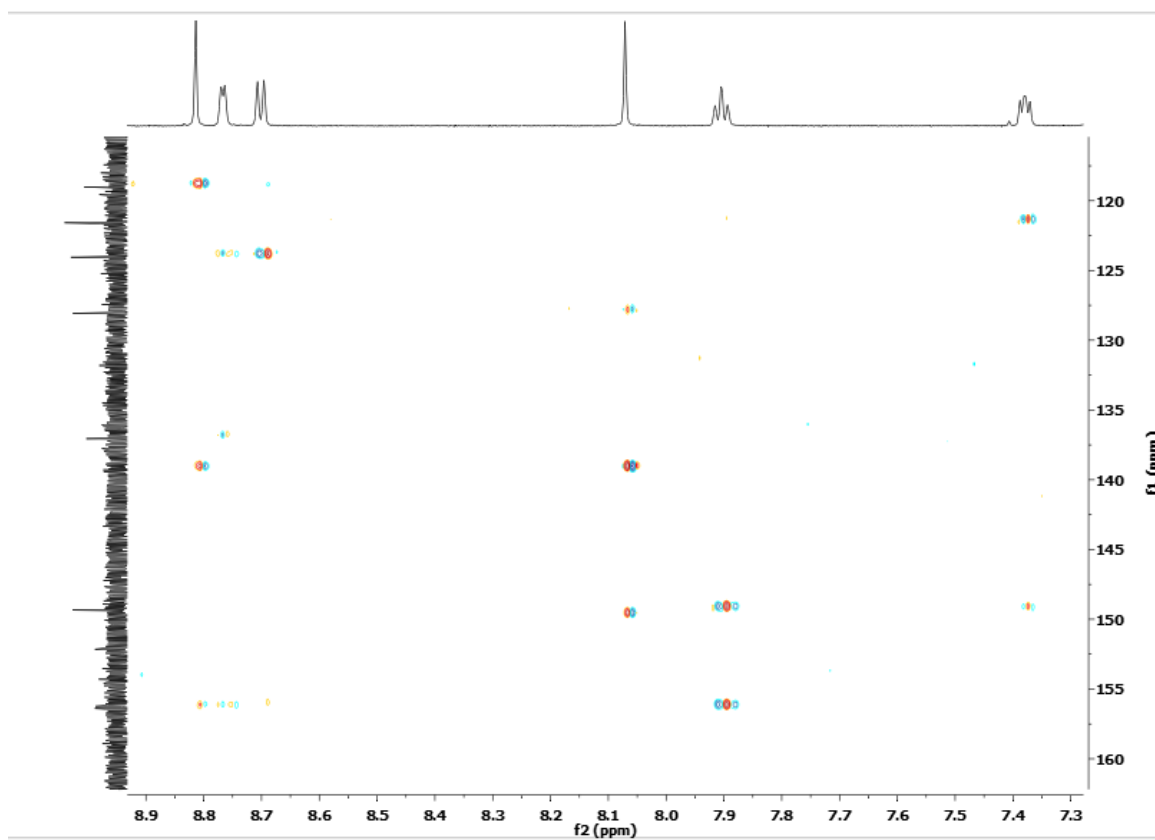
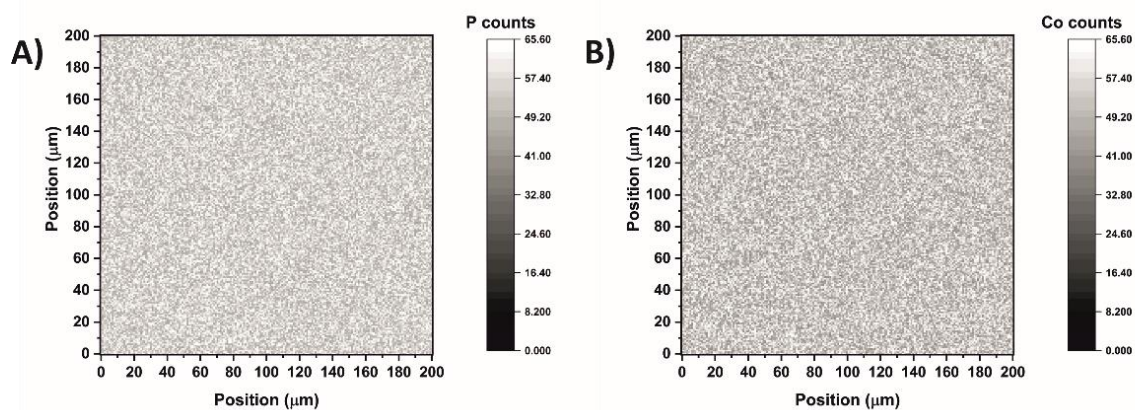


Fig. S4. HMBC NMR in  $\text{CDCl}_3$  of the ditopic ligand  $\text{L}\phi$ .



**Fig. S5.** Secondary Ion Mass Spectrometry analysis of ITO-TPY-Co-TPY electrodes with phosphorous (A) and cobalt (B) atoms.

#### Purification and biochemical characterisation of cytochrome $c_{553}$ 19 AA peptide linker variant

The *petJ* gene encoding for the cytochrome  $c_{553}$  was amplified *via* polymerase chain reaction (PCR) from the *Cyanidioschyzon merolae* genome and genetically modified by adding a 19 amino acid linker and a poly-histidine tag at the C-terminus. The procedure to engineer and express the recombinant cyt protein is described elsewhere<sup>1</sup>. The holoprotein was purified via Immobilized Metal Affinity Chromatography using a HisTrap column and applying a linear 50-500 mM imidazole gradient.<sup>1</sup>

The purity of the cyt  $c_{553}$  protein was confirmed by sodium-dodecyl phosphate gel electrophoresis (see Fig. S6A). The presence of the His<sub>6</sub>-tag was confirmed by Western blot analysis using a His-Probe chemiluminescent detection system (see Fig. S6B). The redox activity of the purified holoprotein was confirmed with a redox difference absorption spectroscopy, using a UV-VIS Shimadzu UV 1800 spectrophotometer. The holoprotein was chemically reduced with sodium dithionite and then oxidized with ferrocyanide in a standard phosphate buffer (pH 7) at room temperature.<sup>1</sup> The spectra were measured for the reduced and oxidized cyt samples, as shown in Fig. S6C.

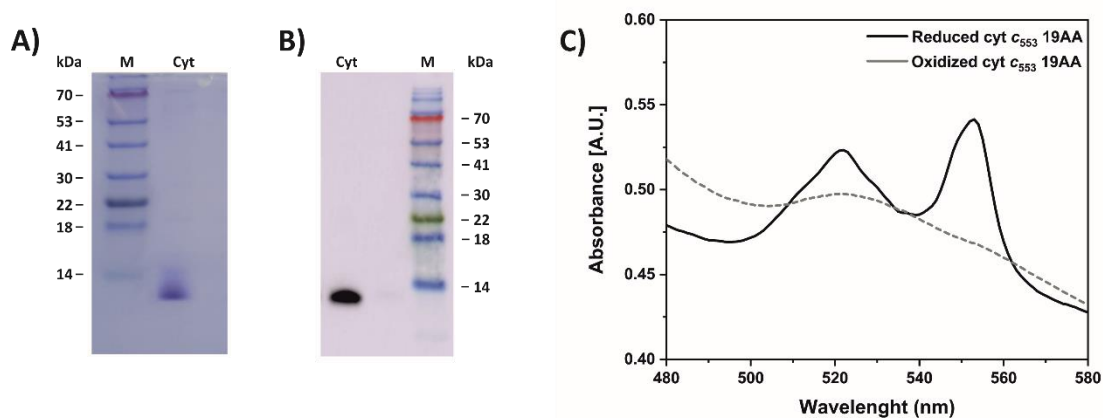


**Fig. S6.** Biochemical characterisation of purified His<sub>6</sub>-tagged cyt  $c_{553}$  19 amino acid variant. **A)** SDS-PAGE analysis shows the purified profile of the cyt  $c_{553}$ . **B)** Western Blot analysis on PVDF membrane. The His<sub>6</sub>-tag at the C-terminus of the holoprotein was detected using the HisProbe system. M, protein pre-stained size marker; cyt, cytochrome  $c_{553}$  19 AA variant (1.5  $\mu$ g protein per lane). **C)** Redox difference adsorption spectroscopy analysis of the pure cyt  $c_{553}$  sample. The UV-VIS spectrum of the reduced sample is shown in black ( $\lambda_{max}$  = 521 nm and 553 nm), while the spectrum of the oxidized cyt sample is depicted with a dashed grey line.

<sup>1</sup>J. D. J. Olmos, P. Becquet, D. Gront, J. Sar, A. Dąbrowski, G. Gawlik, M. Teodorczyk, D. Pawlak and J. Kargul, *RSC Adv.*, 2017, **7**, 47854–47866.

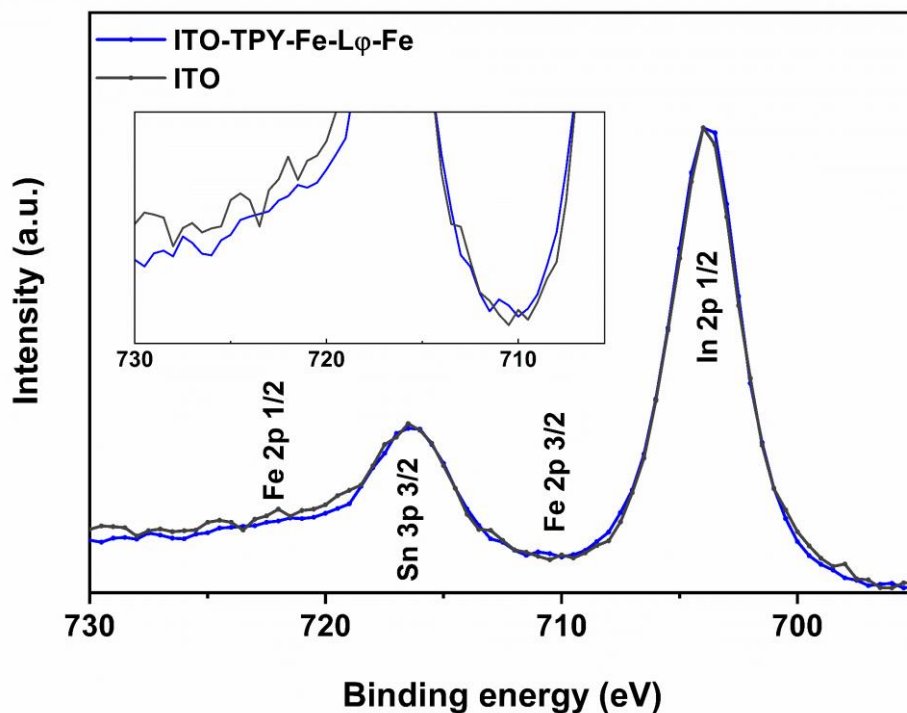


**Fig. S7.** Comparison of XP spectra registered for ITO and ITO-TPY-Fe-L $\phi$ -Fe samples. Strong In  $3p_{1/2}$  and Sn  $3p_{3/2}$  signals mask the potential Fe  $2p$  signals. Inset shows the enlargement of the region where the Fe  $2p$  signals are expected.

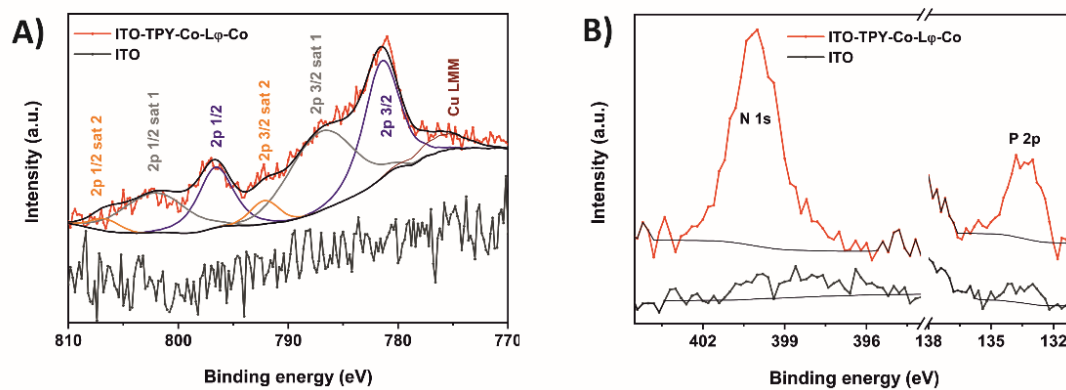


**Fig. S8. A)** XPS analysis of ITO and ITO-TPY-Co-L $\phi$ -Co samples in the Co  $2p$  region. For the Co-TPY spectrum Shirley background had been subtracted before linear background was applied. **B)** Comparison of N  $1s$  and P  $2p$  regions for ITO and ITO-TPY-Co-L $\phi$ -Co samples.

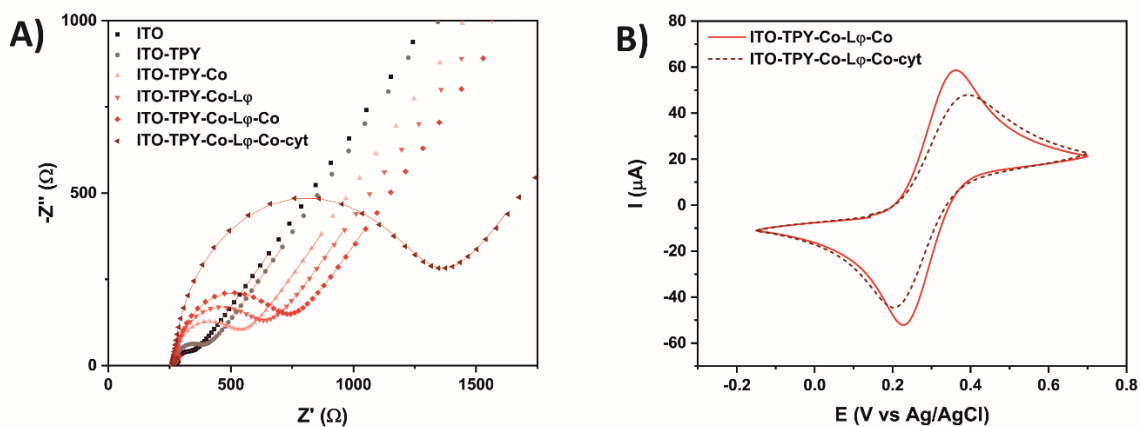


**Fig. S9.** (A) Nyquist plot with fitted curves of impedance spectra obtained for cobalt-based ITO electrodes at different stages of functionalisation. (B) Cyclic voltammetry of ITO-TPY-Co-Lφ-Co and ITO-TPY-Co-Lφ-Co-cyt at 100 mV/s. All measurements were performed with 1 mM 1,1'-ferrocenedimethanol in 0.1 M phosphate buffer (pH 7) under dark conditions.

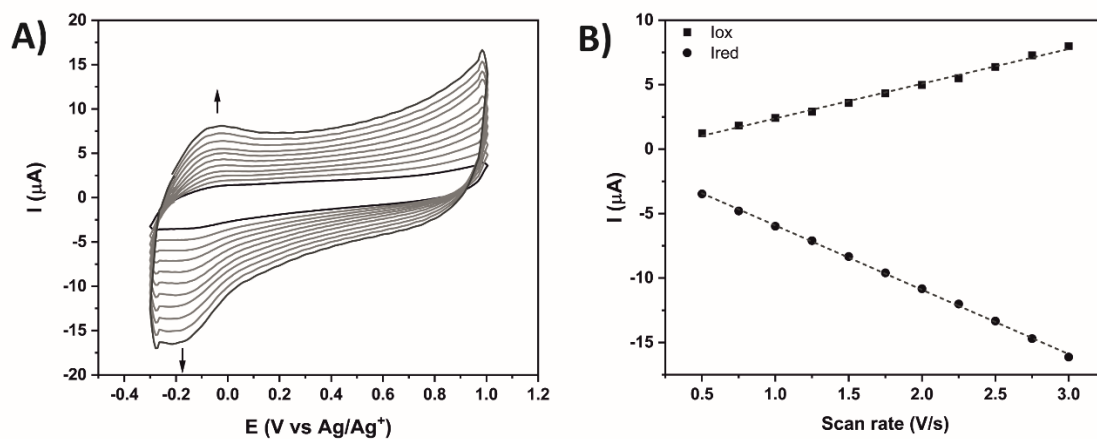


**Fig. S10.** (A) Cyclic voltammetry of ITO-TPY-Co-Lφ at different scan rates from 500 mV/s to 3 V/s in CH<sub>3</sub>CN + 0.1 M HFPTBA. (B) Linear relation between current peak and scan rate obtained for ITO-TPY-Co-Lφ.

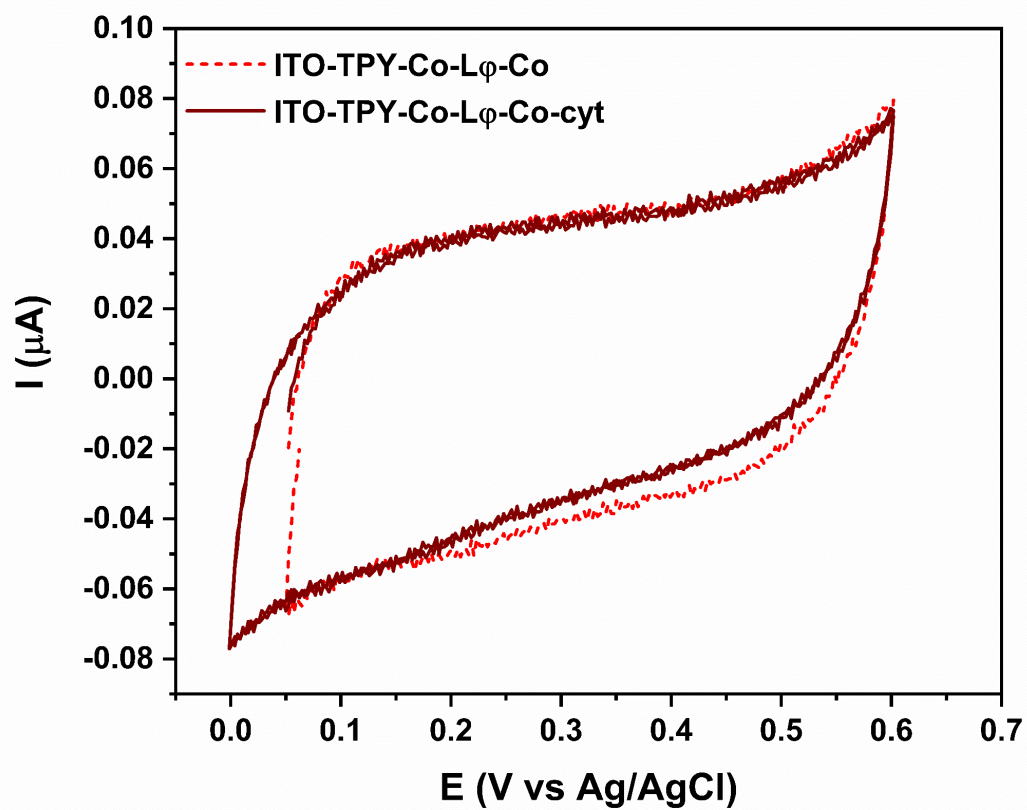


**Fig. S11.** Cyclic voltammetry at 5 mV/s in 0.1 M phosphate buffer (pH 7) of ITO Co-based electrodes without and with immobilised cytochrome.

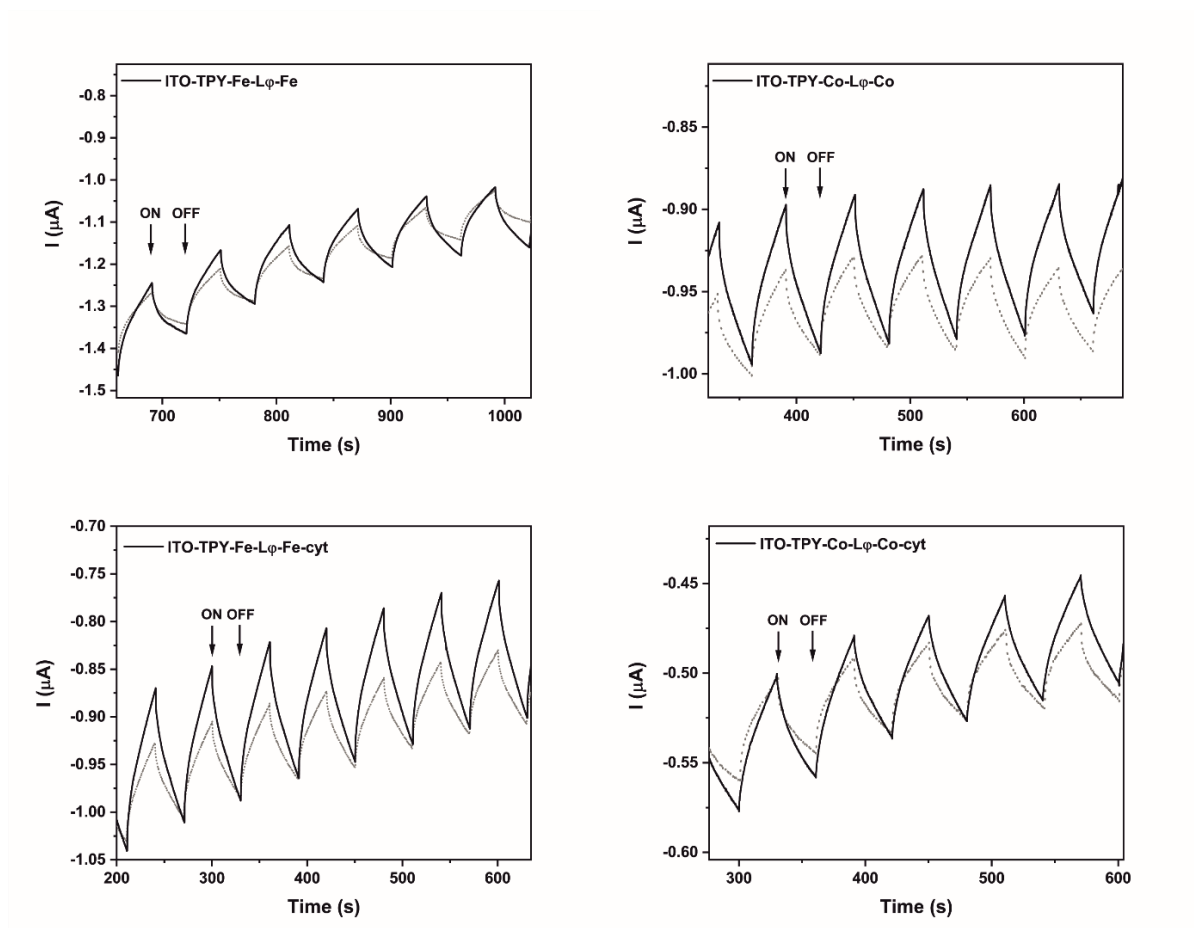


**Fig. S12.** Photochronoamperometry measurements of different TPY-based nanoassemblies in the presence (black) or absence (grey) of  $\text{O}_2$ . The experiments were performed at  $-300$  mV vs Ag/AgCl with 30s. 'light ON/OFF' periods in 5 mM phosphate buffer (pH 7).